



## OPEN ACCESS

## EDITED BY

Yukari Nakano,  
Nidek Co., Ltd., Japan

## REVIEWED BY

Yasuo Terasawa,  
Nidek Co., Ltd., Japan  
Tomomitsu Miyoshi,  
Osaka University, Japan

## \*CORRESPONDENCE

Yong Sook Goo,  
✉ ysgoo@chungbuk.ac.kr

## †PRESENT ADDRESSES

Seongkwang Cha,  
Department of Physiology, Korea University  
College of Medicine, Seoul, Republic of Korea;  
Neuroscience Research Institute, Korea  
University College of Medicine, Seoul, Republic  
of Korea

†These authors have contributed equally to this  
work and share first authorship

RECEIVED 17 April 2024

ACCEPTED 10 July 2024

PUBLISHED 31 July 2024

## CITATION

Yoo Y, Cha S and Goo YS (2024), Comparison of  
modulation efficiency between normal and  
degenerated primate retina.  
*Front. Cell Dev. Biol.* 12:1419007.  
doi: 10.3389/fcell.2024.1419007

## COPYRIGHT

© 2024 Yoo, Cha and Goo. This is an open-  
access article distributed under the terms of the  
[Creative Commons Attribution License \(CC BY\)](https://creativecommons.org/licenses/by/4.0/).  
The use, distribution or reproduction in other  
forums is permitted, provided the original  
author(s) and the copyright owner(s) are  
credited and that the original publication in this  
journal is cited, in accordance with accepted  
academic practice. No use, distribution or  
reproduction is permitted which does not  
comply with these terms.

# Comparison of modulation efficiency between normal and degenerated primate retina

Yongseok Yoo<sup>1†</sup>, Seongkwang Cha<sup>2†‡</sup> and Yong Sook Goo<sup>2,3\*</sup>

<sup>1</sup>School of Computer Science and Engineering, Soongsil University, Seoul, Republic of Korea,

<sup>2</sup>Department of Physiology, College of Medicine, Chungbuk National University, Cheongju, Republic of Korea, <sup>3</sup>Biomedical Research Institute, Chungbuk National University Hospital, Cheongju, Republic of Korea

With electrical stimulation, retinal prostheses bypass dysfunctional photoreceptors and activate the surviving bipolar or retinal ganglion cells (RGCs). Therefore, the effective modulation of RGCs is crucial for developing retinal prostheses. Substantial research has been performed on the ability of an electrical stimulus to generate a reliable RGC response. However, different experimental conditions show varying levels of how well the electrical stimulation evokes RGC spikes. Therefore, in this study, we attempted to extract an indicator to understand how the electrical stimulation effectively evokes RGC spikes. Six cynomolgus monkeys were used: three as controls and three as an N-methyl-N-nitrosourea (MNU)-induced retinal degeneration model. The retinal recordings were performed using 8 × 8 multi-electrode arrays (MEAs). Electrical stimulation consisted of symmetrical biphasic pulses of varying amplitudes and durations. The number of stimulation conditions that resulted in significantly higher post-stimulation firing rates than pre-stimulus firing rates was defined as the modulation efficiency ratio (MER). The MER was significantly lower in degenerated retinas than in normal retinas. We investigated the relationship between the variables and the MER in normal and degenerated primate RGCs. External variables, such as duration and inter-electrode distance, and internal variables, such as average firing rates and statistics (mean, standard deviation, and coefficient of variation [CV]) of inter-spike intervals (ISIs) of spontaneous spikes, were used. External variables had similar effects on MER in normal and degenerated RGCs. In contrast, internal variables affected MER differently in normal and degenerated RGCs. While in normal RGCs, they were not related to MER, in degenerated RGCs, the mean ISIs were positively correlated with MER, and the CV of ISIs was negatively correlated with MER. The most important variable affecting MER was the mean ISI. A shorter ISI indicates hyperactive firing in the degenerated retina, which prevents electrical stimulation from evoking more RGCs. We believe that this hyperactivity in degenerated retinas results in a lower MER than that in the normal retina. Our findings can be used to optimize the selection of stimulation channels for *in vitro* MEA experiments and practical calibration methods to achieve higher efficiency when testing retinal prostheses.

## KEYWORDS

retinal prosthesis, retinal ganglion cell, electrical stimulation, spontaneous firing, inter-spike interval, modulation efficiency

# 1 Introduction

Retinal prostheses have been the subject of extensive research (Humayun et al., 2012; Lorach et al., 2015; Stingl et al., 2015; Fujikado et al., 2016; Weiland et al., 2016; Ayton et al., 2020). These medical devices replace the function of dead or dysfunctional photoreceptors. An epiretinal prosthesis can function by applying direct electrical stimulation to the surviving bipolar cells (BCs) or retinal ganglion cells (RGCs), whereas subretinal prostheses utilize incident light to trigger electrical stimulation via photodiodes (Lorach et al., 2015; Stingl et al., 2015). Ongoing research and development efforts aim to improve the efficacy, resolution, safety, and overall impact on the quality of life of individuals with visual impairments.

The development of retinal prostheses requires knowledge of how retinal neurons respond to electrical stimulation. The bipolar and ganglion cells are the main targets of electrical stimulation. The effect of electrical stimuli on the retina is most often determined by recording the responses of ganglion cells *in vitro* (Jensen et al., 2003; Jensen et al., 2005; Fried et al., 2006; Jensen and Rizzo, 2008; Sekirnjak et al., 2008; Jensen and Rizzo, 2009; Goo et al., 2011a; Jepson et al., 2013; Ahn et al., 2015; Weitz et al., 2015; Ahn et al., 2022; Ahn et al., 2023; Cha et al., 2023; Gogliettino et al., 2023). Consequently, electrical stimuli are classified according to their mechanism of action on RGCs into direct and indirect (network-mediated) stimulations. Direct stimulation of RGCs refers to a stimulus that depolarizes the ganglion cell membrane, causing RGCs to fire a spike without presynaptic input. Direct stimulation of RGCs causes them to fire a spike within a millisecond of the stimulus presentation (Sekirnjak et al., 2006; Jepson et al., 2013). Although direct stimulation can control RGC activity with fine temporal precision, axonal stimulation often makes it difficult to achieve a high spatial resolution (Weitz et al., 2013; Weitz et al., 2015). The indirect stimulation of RGCs is achieved by stimulating BCs, which in turn activate postsynaptic ganglion cells. The rationale for indirect stimulation is that the remaining retinal circuitry processes and refines the stimulus to produce a more natural ganglion cell output that mimics the physiological response. Therefore, our group has focused on the indirect stimulation of RGCs (Ahn et al., 2022; Cha et al., 2022; Ahn et al., 2023; Cha et al., 2023).

Substantial research has been performed on the ability of an electrical stimulus to generate a reliable RGC response in terms of the electrode location and the stimulus parameters, such as stimulus amplitude, duration, frequency, and pulse shape.

Epiretinal cathodic stimulation of ganglion cells has lower thresholds than anodic stimulation (Jensen et al., 2005; Ahn et al., 2015). Subretinal anodic stimulation has lower ganglion cell thresholds than cathodic stimulation has (Boinagrov et al., 2014). RGCs are most responsive to fast voltage changes to 1,000 Hz stimulation, while low-frequency (5–25 Hz) sinusoids can activate BCs, avoiding the activation of underlying ganglion cell axons (Freeman et al., 2010; Grosberg et al., 2017). BCs are known to be more responsive to 100 Hz stimulation, whereas photoreceptors are more responsive to 10 Hz stimulation (Freeman et al., 2010; Twyford and Fried, 2016). From the strength-duration curve, the rheobase current and chronaxie can be derived. For ganglion cells, chronaxie, which is the stimulus pulse

duration found at twice the rheobase current, has been measured to be between 0.08 and 0.6 ms (Jensen et al., 2005; Sekirnjak et al., 2006; Ahuja et al., 2008; Eickenscheidt et al., 2012; Weiland et al., 2016).

Previous research greatly improves our understanding of how to generate reliable RGC responses with electrical stimulation. However, all the information is constrained by the experimental conditions, such as animal species, electrode configuration, electrical stimulation pulse, and so on. Sekirnjak et al. (2006) thoroughly reviewed all the preceding *in vitro* and *in vivo* experiments regarding animal species, electrodes, stimulation pulses, and threshold values. However, the comparison of different experiments makes it difficult to demonstrate how well electrical stimulation evokes RGC spikes. Therefore, in this study, we attempted to extract an indicator of modulation efficiency of an RGC, to quickly understand how electrical stimulation effectively evokes RGC spikes.

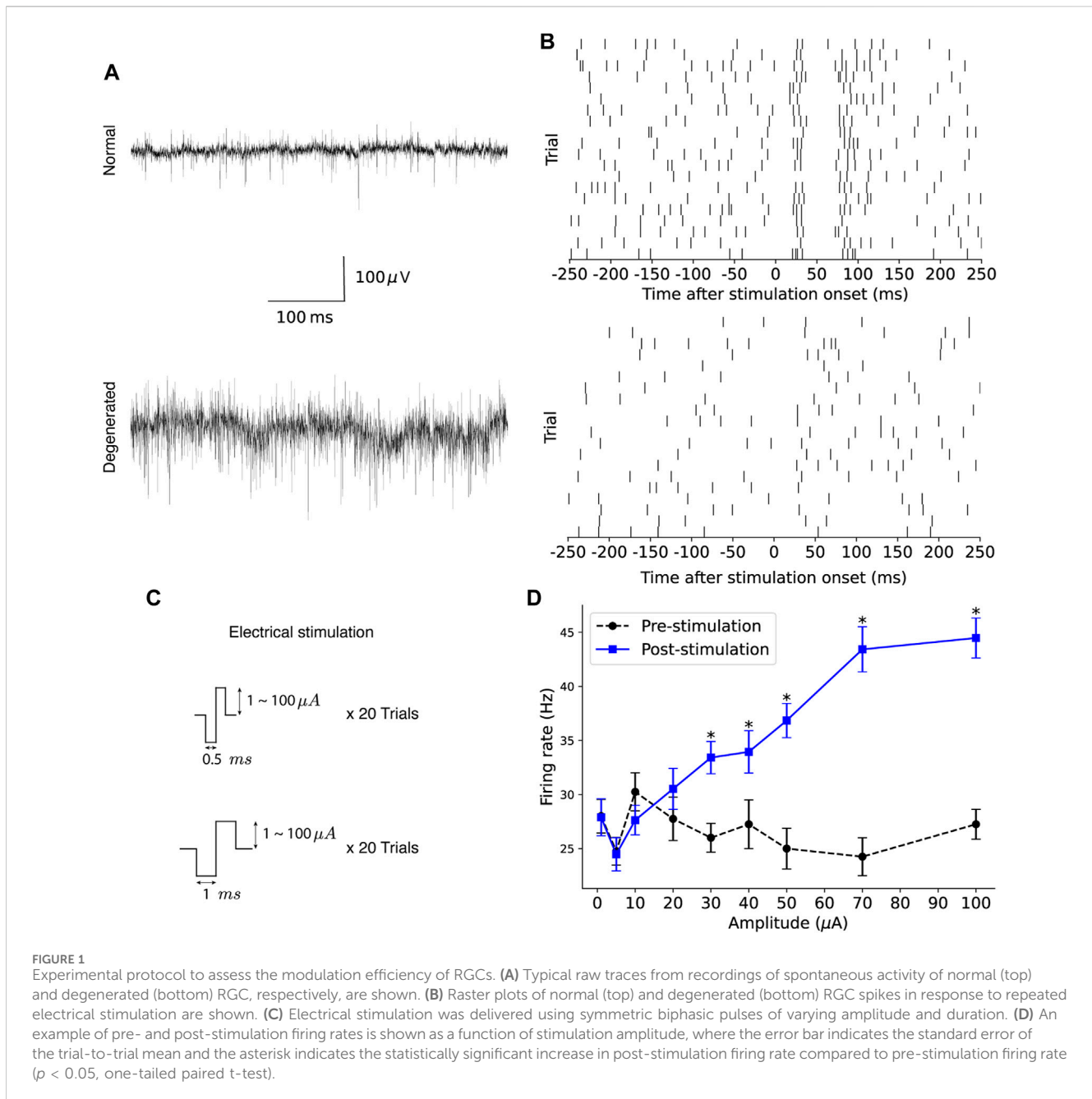
Specifically, we examined the effects of external and internal variables on the modulation efficiency in activating normal and degenerated primate RGCs using a 64-channel multi-electrode array (MEA). External variables include how the electrical current is delivered to an RGC, such as the charge of the electrical stimulation and the physical distance between the stimulating and recording electrodes. For internal variables, we focused on the intrinsic properties of an RGC that can be measured extracellularly. Spontaneous spiking patterns prior to electrical stimulation were summarized as internal variables.

Electrical stimulation studies with normal primate retinas related to retinal prostheses have been performed because the non-human primate (NHP) retina is the best animal model to mimic the human retina (Sekirnjak et al., 2008; Jepson et al., 2013; Gogliettino et al., 2023). However, to the best of our knowledge, there are no reports except our previous publication (Cha et al., 2023) that compared normal and degenerated NHP RGC related to retinal prostheses. The use of a drug-induced primate degeneration model in this study provided a unique opportunity to explore the differences between normal and degenerated RGCs in terms of modulation efficiency. The controlled environment of the *in vitro* setting allowed for a detailed analysis of how various factors influence the excitability and modulation of RGCs, providing insights that may contribute to the development of more effective retinal prostheses and treatments for vision restoration.

## 2 Materials and methods

### 2.1 Animals

Retinas were obtained from six adult male Cynomolgus monkeys (*Macaca fascicularis*). Retinal degeneration was induced in three monkeys by injecting them with N-methyl-N-nitrosourea (MNU) 14–21 weeks before sacrifice. We have previously reported the detailed procedures for drug-induced retinal degeneration and their confirmation (Choi et al., 2023). The remaining three monkeys served as controls. All procedures were performed in compliance with the ARRIVE guidelines. This study was approved by the Institutional Animal Care and Use Committee of Osong Medical



Innovation Foundation, Cheongju, Republic of Korea (KBIO-IACUC-2020-054-4).

The retinas were cut into approximately 2 mm × 2 mm patches and mounted on an MEA (60pMEA200/30iR-Ti, Multichannel Systems GmbH, Reutlingen, Germany) with the ganglion cell layer facing down. The retinal patches' eccentricity for MEA recording was 4~8 mm from the fovea as shown in our previous publication [Figure 1 of Cha et al. (2023)]. All the patches were placed in an artificial cerebrospinal fluid solution (124 mM NaCl, 10 mM glucose, 1.15 mM  $\text{KH}_2\text{PO}_4$ , 25 mM  $\text{NaHCO}_3$ , 1.15 mM  $\text{MgSO}_4$ , 2.5 mM  $\text{CaCl}_2$ , and 5 mM KCl, all purchased from Sigma-Aldrich, St. Louis, MO, United States), bubbled with 95%  $\text{O}_2$  and 5%  $\text{CO}_2$  to maintain a pH of 7.3–7.4 at 25°C under near-infrared (IR) illumination.

## 2.2 *In vitro* recording and stimulation

The MEA contained 64 circular electrodes in an 8 × 8 grid layout with electrode diameters of 30  $\mu\text{m}$  and interelectrode distances of 200  $\mu\text{m}$ . The electrodes were coated with porous titanium nitride and embedded in a perforated polyimide foil that provided sufficient oxygen and nutrient supply to the retina. Recordings of retinal activity were obtained from multielectrodes with a bandwidth ranging from 1 to 3,000 Hz at a gain of 1,200. The data-sampling rate was 25 kHz for each electrode.

After waiting 20 min for the retinal tissue on the MEA to stabilize, spontaneous RGC responses were recorded without electrical stimulation for approximately 30 s. Figure 1A shows typical raw traces from normal (top) and degenerated (bottom)

RGC recordings. Electrical stimulation generated by a stimulus generator (STG 1004, Multichannel Systems GmbH, Reutlingen, Germany) was applied to the retinal patch through one electrode, while the other 58 electrodes recorded the RGCs extracellularly. Figure 1B shows the raster plots of the normal RGC (top) and the degenerated RGC (bottom) in response to repeated trials.

Electrical stimulation consisted of symmetrical biphasic pulses of varying amplitudes and durations (Figure 1C). Pulse duration was either 0.5 or 1 ms, and pulse amplitudes of 1, 5, 10, 20, 30, 40, 50, 70, and 100  $\mu$ A were applied for each duration, resulting in total 18 stimulation conditions. Biphasic current pulses were applied 20 times, once per second (1 Hz), for each stimulation condition.

## 2.3 Data analysis

The spike times of the RGCs were preprocessed as follows: The raw MEA recording trace was high-pass filtered with a cutoff frequency of 100 Hz, and spike sorting was performed on the filtered signal using Offline Sorter™ v4 (Plexon Inc., Dallas, TX, United States) to transform the waveforms containing multiunit activities into multiple single-unit spike trains. The total number of identified cells was 530 normal RGCs and 360 degenerated RGCs. The resulting time stamps of the RGC spikes were analyzed using custom Python codes developed in-house.

Spontaneous firing activity during the 30-second period was quantified as follows: First, the average spontaneous firing rates were calculated. Next, inter-spike intervals (ISIs) were calculated for all spontaneous spikes. The mean and standard deviation of the ISIs were then calculated for ISIs of less than 500 ms.

To focus on the network-mediated RGC responses, we collected the spikes originating from soma of RGCs by electrical stimulation and excluded the axon-stimulating response as follows. First, we used a post-stimulation time window after 10 ms to exclude the stimulus artifact or the direct RGC response occurring within 10 ms after stimulus onset (Sekirnjak et al., 2006; Boinagrov et al., 2014; Ahn et al., 2017). Second, we removed spikes with triphasic waveforms to exclude the recordings from RGC axons far from the stimulating point. This is because spikes recorded from electrodes close to axons in the macaque retina show a typical waveform of triphasic rather than biphasic temporal structure and smaller amplitude spikes than soma stimulation (Madugula et al., 2022).

The modulation efficiency for the electrically evoked spikes was quantified as follows. First, for each electrical stimulation, firing rates were measured for the pre-stimulation (−200~0 ms) and post-stimulation (10~200 ms) time windows, denoted by  $FR_{pre}$  and  $FR_{post}$ , respectively. Then, reliable modulation of RGCs by electrical stimulation is determined by whether the post-stimulation firing rate is significantly greater than the pre-stimulation firing rate. Specifically, for each stimulation condition, the significance of the increase in firing rate from pre-stimulation to post-stimulation was quantified using the one-tailed paired t-test for 20 trials of  $FR_{pre}$  and  $FR_{post}$  with a significance  $p$ -value of 0.05. For levels of stimulation amplitude ( $n_{amplitude}$ ), the number of such significant increases in firing rate is counted and denoted by  $n_{significance}$ . Finally, the ratio of  $n_{significance}$  to  $n_{amplitude}$  is defined as modulation efficiency ratio (MER) in Eq. 1.

TABLE 1 Linear regression of MER onto external and internal variables (n.s.:  $p > 0.05$ , \*\*\*:  $p < 0.001$ , \*\*:  $p < 0.01$ , \*:  $p < 0.05$ ).

Group	Estimated coefficient	
	Normal	Degenerated
Inter-electrode distance	−0.002***	−0.002***
Spontaneous firing rate	−0.0006 <sup>n.s.</sup>	−0.0024 <sup>n.s.</sup>
Mean of ISI	0.0003 <sup>n.s.</sup>	0.0012***
The standard deviation of ISI	0.0004 <sup>n.s.</sup>	0.0009*
CV <sub>ISI</sub>	−0.08 <sup>n.s.</sup>	−0.28**

ISI, inter-spike interval; CV, coefficient of variation; n.s., no significance.

$$MER = \frac{n_{significance}}{n_{amplitude}}. \quad (1)$$

Figure 1D shows an example of the pre- and post-stimulation firing rates as a function of stimulation amplitude. Black circles with dotted lines indicate the trial-to-trial mean pre-stimulation firing rates. Blue squares with solid lines indicate the trial-to-trial mean post-stimulation firing rates, with the error bar indicating the standard error of the trial-to-trial mean. Both pre- and post-stimulation firing rates showed high trial-to-trial variability. The pre-stimulation firing rates fluctuated for different current amplitudes. In addition, the post-stimulation firing rates were close to or even lower than the corresponding pre-stimulation firing rates when the stimulation amplitude was low. Among nine stimulation amplitude values ( $n_{amplitude} = 9$ ), the post-stimulation firing rate was significantly greater than the pre-stimulation firing rate for the five stimulation amplitudes ( $n_{significance} = 5$ ), indicated by asterisks in Figure 1D. Thus, MER was 5/9 for this example.

If there were more than two modes in the given histogram (Figure 3B), the centers of the modes were calculated using the Gaussian mixture model (Parsons, 2020). Specifically, the k-means clustering algorithm (MacQueen, 1967; Jain, 2010) was used to obtain an initial estimate of the centers. The centers were then iteratively updated using the expectation-maximization algorithm (Dempster et al., 1977; Xu and Jordan, 1996) until convergence.

For the analysis of the bimodal histograms of MER shown in Figure 4B, if the given histogram was bimodal, the threshold separating the two modes was determined using the Otsu algorithm (Otsu, 1979) as follows: First, the within-class variance values were calculated for all possible thresholds. For instance, the number of significant increase (numerator of the MER) can take integer values ranging from zero to eight. Therefore, the possible threshold values are 0.5/9, 1.5/9, . . . , and 8.5/9. Next, the threshold that minimized the within-class variance was chosen as the optimal threshold.

For the analysis of the ISIs shown in Figure 7, histograms of the ISIs were fitted as follows: For normal RGCs, histograms of ISIs were fitted with a gamma distribution, which models the exponential decay and the refractory periods (Dayan and Abbott, 2005). Degenerated RGCs tended to show an additional peak in the ISI histogram at approximately 50 ms, corresponding to spikes synchronized with the oscillatory rhythms in degenerated retinal

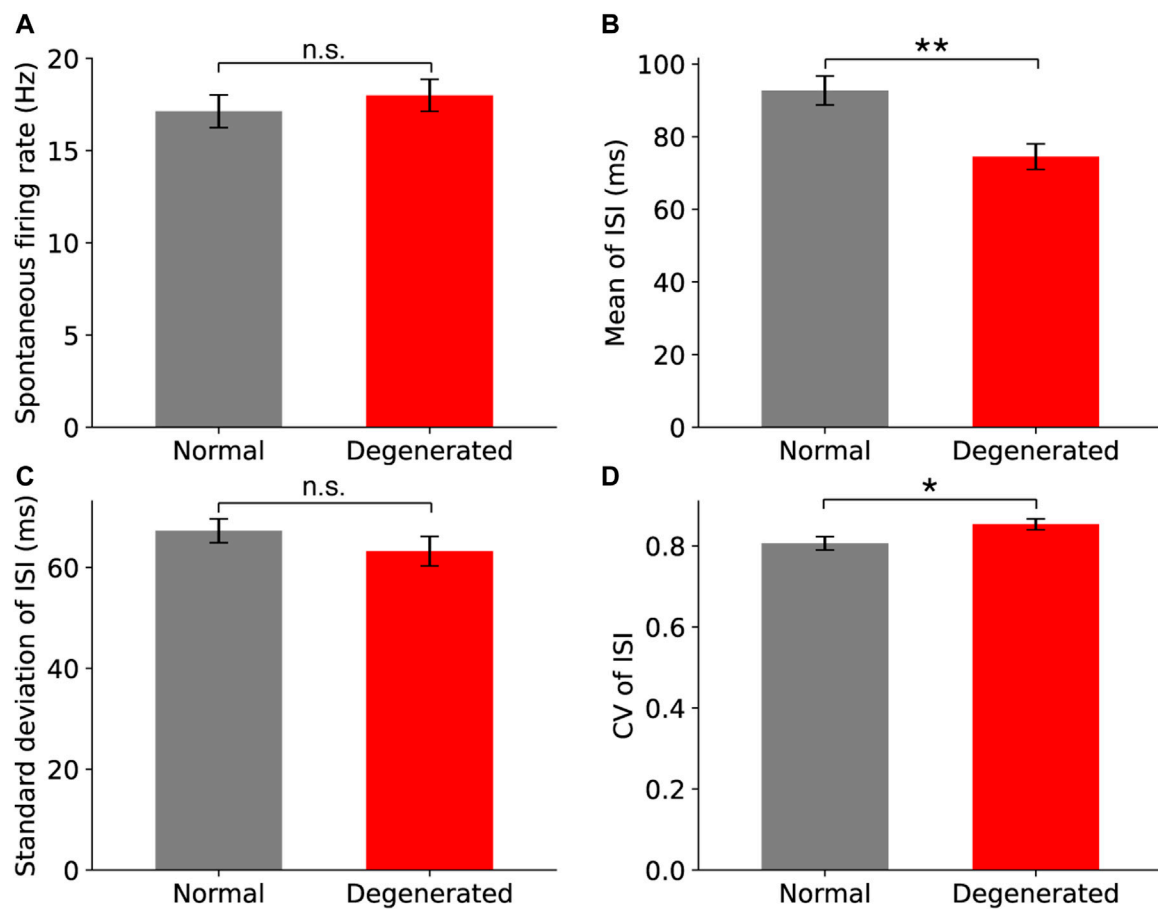


FIGURE 2

Comparison of spontaneous firing properties between normal (gray) and degenerated (red) RGCs for spontaneous firing rate (A), the mean ISI (B), the standard deviation of ISI (C), and the coefficient of variation (CV) of ISI (D). The error bar represents the standard error of the mean. Statistical significance was assessed using the t-test; asterisks and n.s. represent statistical significance (\*\*:  $p < 0.01$ , \*:  $p < 0.05$ ) and no significance ( $p > 0.05$ ), respectively.

networks (Goo et al., 2016; Ahn et al., 2022). Therefore, the ISI histogram of the degenerated RGCs was fitted using a mixture of gamma and Gaussian distributions.

The association between the predictors of interest and the MER was evaluated (Table 1). Linear regression was performed using internal and external variables as predictors. The statistical significance of the association between a given predictor and MER was assessed at a significance level of 0.05. The null hypothesis was that there was no association between the predictor and MER (coefficient = 0). If the  $p$ -value of the coefficient was  $< 0.05$ , the null hypothesis was rejected, indicating that changes in the predictor were significantly associated with MER.

### 3 Results

#### 3.1 Comparison of spontaneous firing properties between normal and degenerated RGCs

Among the four internal variables of spontaneous firing, the mean and CV of the ISIs were significantly different between normal and

degenerated RGCs. The spontaneous firing properties of normal (gray) and degenerated (red) RGCs are compared in Figure 2. Spontaneous firing rates measured for 30 s did not differ between normal and degenerated RGCs ( $p > 0.05$ , t-test; Figure 2A). In contrast, the mean ISI of the degenerated RGCs was significantly shorter than that of the normal RGCs (\*\* $p < 0.01$ , t-test; Figure 2B). Thus, degenerated RGCs tended to generate more spikes within a shorter time interval than normal RGCs did. The standard deviations (SDs) of ISI did not differ between normal and degenerated RGCs (n.s.:  $p > 0.05$ , t-test; Figure 2C). The CV of the ISI of the degenerated RGCs was higher than that of the normal RGCs (\* $p < 0.05$ , t-test; Figure 2D). This is because CV is the ratio of the SDs to the mean. A lower mean ISI and the same SDs resulted in a higher CV.

Figure 3 shows the histograms of the two internal variables that showed significant differences between the normal and degenerated RGCs. Figure 3A shows the histograms of the mean ISI of normal (gray) and degenerated (red) RGCs. First, the normal RGCs (gray) had a wider range of mean ISIs than the degenerated RGCs (red) had. Secondly, degenerated RGCs were more likely to have shorter mean ISIs ( $< 0.15$  s) and less likely to have longer mean ISIs ( $> 0.15$  s) than normal RGCs were. Consequently, the distributions of mean ISIs were significantly different between normal and degenerated RGCs ( $p < 0.05$ , Mann-Whitney U test).

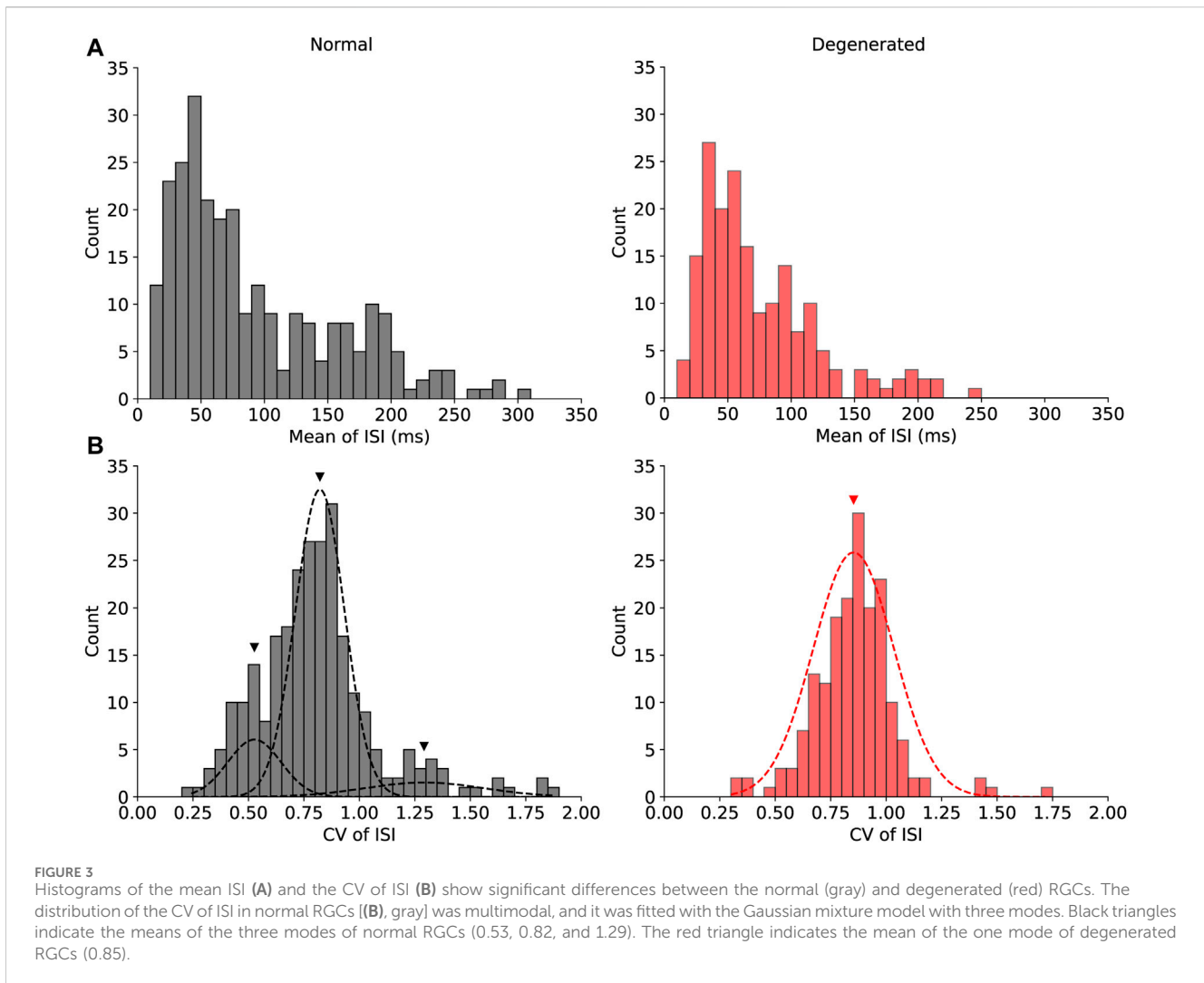


Figure 3B shows histograms of the CV of the ISI for normal (gray) and degenerated (red) RGCs. The distributions of the CV of ISI were significantly different between the normal and the degenerated RGCs ( $p < 0.001$ , Mann-Whitney U test). In particular, the distribution of the CV of the ISI in normal RGCs was multimodal. Figure 3B shows the three modes of the normal RGC distributions fitted with the Gaussian mixture model as black dashed curves, with black triangles indicating the centers of the three modes. The middle mode (mean = 0.82) of the normal RGCs was the most common, followed by the lower (mean = 0.53) and upper (mean = 1.29) modes. In contrast, the CV of the ISI of the degenerated RGCs had a unimodal distribution with a mean of 0.85 and was marked by a red triangle, which was close to the main mode of normal RGCs. Thus, the degenerated RGCs showed less diversity with respect to the CV of the ISI.

### 3.2 Assessment of modulation efficiency of normal vs. degenerated RGCs

The degenerated RGCs had lower MER than normal RGCs had. Figure 4A shows the MER of normal (gray) and degenerated (red) RGCs, with error bars representing the standard error of the mean (SEM). The

mean MER of each group was 3.8/9 (normal) and 2.8/9 (degenerated). The difference between the means was statistically significant ( $p < 0.001$ , t-test).

Furthermore, the MER of both normal and degenerated RGCs showed a bimodal distribution. Figure 4B shows histograms of the MER of normal (gray) and degenerated (red) RGCs when the stimulation duration was 0.5 ms. The optimal threshold that separates MER values into two classes was 3.5/9 for both normal and degenerated RGCs. Thus, the high MER region is shown in the green region in Figure 4B.

Figure 4C shows the proportions of MER with a stimulation duration of 0.5 ms for each group. Fewer degenerated RGCs had higher MER than the normal group had. For the normal RGCs, 54% had an MER greater than 3.5/9 (Figure 4C, left). For the degenerated RGCs, 36% had an MER greater than 3.5/9 (Figure 4C, right).

### 3.3 Effects of external variables on the modulation efficiency of the electrical stimulation

Longer stimulation durations increased MER in both normal and degenerated RGCs, although the degree of increase in MER

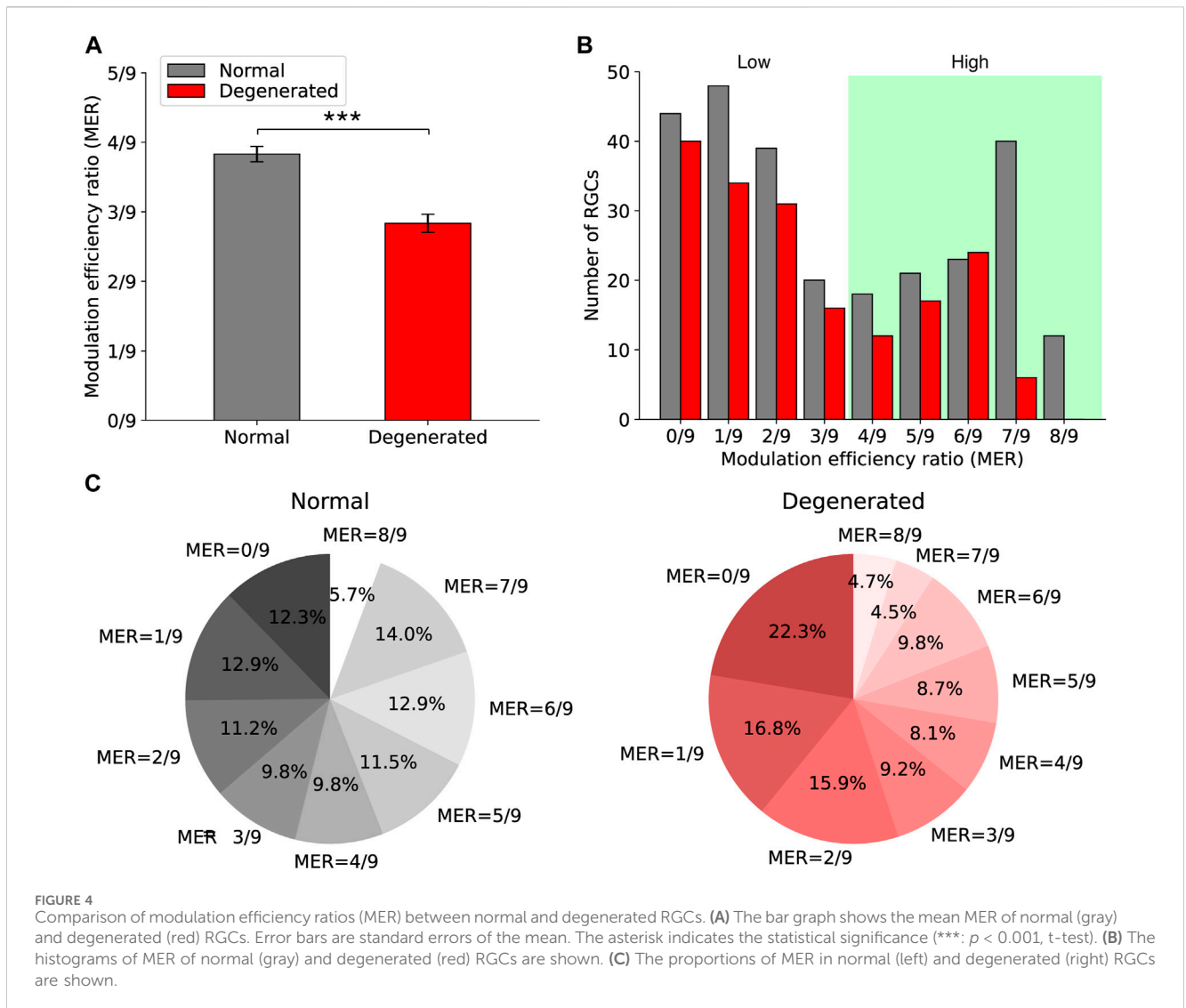


**FIGURE 4** Comparison of modulation efficiency ratios (MER) between normal and degenerated RGCs. **(A)** The bar graph shows the mean MER of normal (gray) and degenerated (red) RGCs. Error bars are standard errors of the mean. The asterisk indicates the statistical significance (\*\*\*:  $p < 0.001$ , t-test). **(B)** The histograms of MER of normal (gray) and degenerated (red) RGCs are shown. **(C)** The proportions of MER in normal (left) and degenerated (right) RGCs are shown.

efficiency differed between the groups. **Figure 5A** shows MER as a function of stimulation duration, with error bars indicating SEM. When stimulation duration was increased from 0.5 to 1 ms, the mean MER of normal RGCs increased from 3.3/9 to 4.4/9 (black circles). This increase was statistically significant (\*\* $p < 0.001$ , t-test), indicating that most RGCs were modulated by a higher charge. T-test was used to assess statistical significance because the stimulation duration had only two values. Similarly, the MER of degenerated RGCs increased from 2.6/9 to 3.1/9 with longer stimulation durations (red squares). This increase was statistically significant (\* $p < 0.05$ , t-test), yet less than that of the normal RGCs. Additionally, the average MER of degenerated RGCs remained below 3.5/9.

MER decreased as the distance between the stimulation and recording electrodes increased. **Figure 5B** shows the MER as a function of the inter-electrode distance, with error bars indicating the SEM. For normal RGCs (black circles), the MER was highest (5.9/9) at the shortest inter-electrode distance (200  $\mu\text{m}$ ) and then decreased as the inter-electrode distance increased. The slope of the linear regression fit (black

dashed line) was  $-0.002 \mu\text{m}^{-1}$  and significantly different from zero (**Table 1**). For degenerated RGCs (red squares), the highest MER (4.6/9) was achieved when the inter-electrode distance was slightly farther (400  $\mu\text{m}$ ). The linear regression fit of the degenerated RGCs (red dashed line) showed a similar slope ( $-0.002 \mu\text{m}^{-1}$ ) to that of the normal RGCs (**Table 1**).

### 3.4 Effects of internal variables on the modulation efficiency of the electrical stimulation

While the internal variables were not associated with MER in normal RGCs, the properties of inter-spike intervals were associated with MER in degenerated RGCs. **Figure 6** shows scatterplots of the MER and internal variables for the normal (black) and the degenerated (red) RGCs, with regression lines (dashed) and 95% confidence regions (shaded). The estimated coefficients of the regression fit are listed in **Table 1**. The relationship between the MER and each internal variable is as follows.

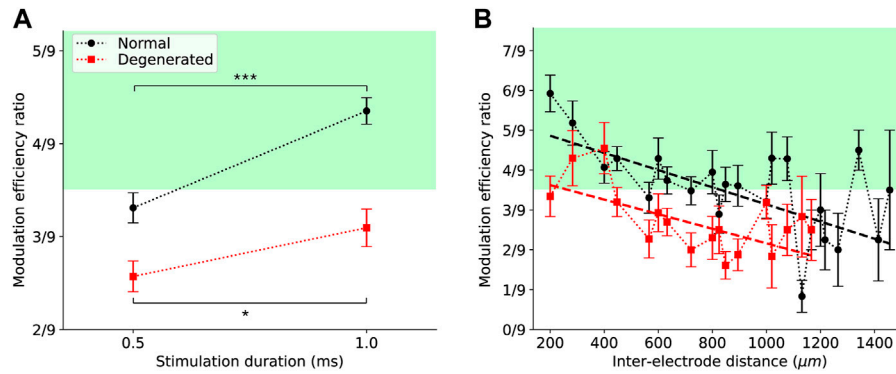


**FIGURE 5** Effects of external variables on the modulation efficiency ratio (MER) of electrical stimulation. **(A)** MER increased for both normal (black) and degenerated (red) RGCs when stimulation duration was increased from 0.5 to 1 ms. Error bars are standard errors of the mean. Asterisks indicate statistical significance ( $p < 0.001$  (\*\*\*) for normal and  $p < 0.05$  (\*) for degenerated, t-test). **(B)** MER tended to decrease with increasing distance between stimulating and recording electrodes for both normal (black) and degenerated (red) RGCs. Error bars represent standard errors of the mean. Dashed lines are linear regression fits.

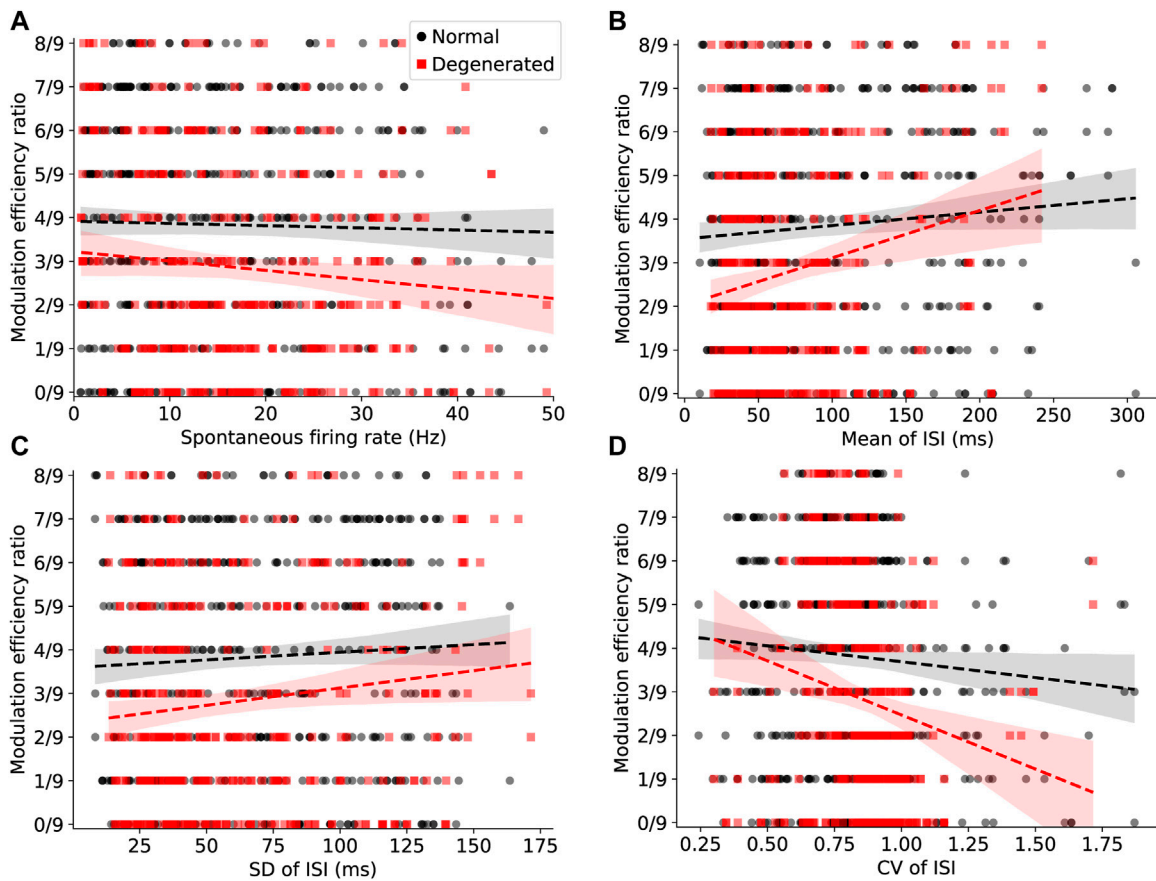


**FIGURE 6** Effects of internal variables on the modulation efficiency of electrical stimulation. Scatter plots of MER and internal variables for normal (black) and degenerated (red) RGCs are shown, with regression lines (dashed) and 95% confidence regions (shaded). **(A)** Spontaneous firing rates of RGCs were not associated with MER for both normal (black) and degenerated (red) RGCs ( $p > 0.05$ , linear regression). **(B)** The mean of the inter-spike interval (ISI) was positively correlated with MER only in degenerated RGCs ( $p < 0.05$ , linear regression) but not in normal RGCs ( $p > 0.05$ , linear regression). **(C)** The standard deviation (SD) of ISI was positively correlated with MER only in degenerated RGCs ( $p < 0.05$ , linear regression) but not in normal RGCs ( $p > 0.05$ , linear regression). **(D)** The CV of ISI was negatively correlated with MER only in degenerated RGCs ( $p < 0.05$ , linear regression) but not in normal RGCs ( $p > 0.05$ , linear regression).

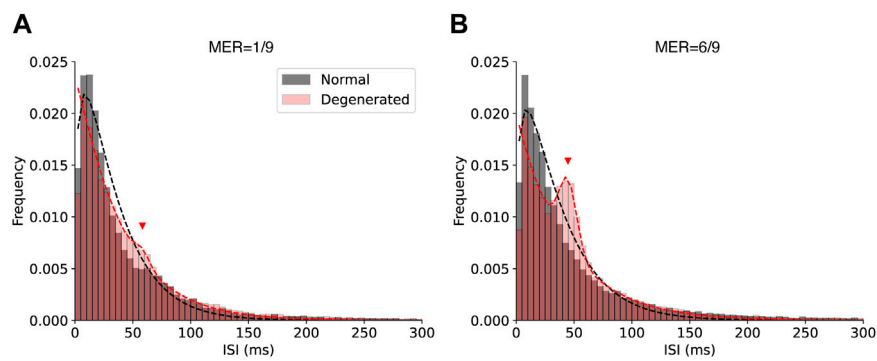


FIGURE 7

Histograms of the ISI of normal (black) and degenerated (red) RGCs with low (A) and high (B) modulation efficiency. Black dashed curves represent gamma distribution fits for the normal RGCs. Red dashed curves represent fits using a mixture of gamma and normal distributions for the degenerated RGCs. Red triangles indicate the additional peak fit by the normal distribution.

Spontaneous firing rates of RGCs were not associated with MER in either the normal or the degenerated RGCs. The regression lines (dashed lines) in Figure 6A show a subtle negative correlation with MER in both normal (black) and degenerated (red) RGCs. However, this correlation is not statistically significant, as demonstrated by the  $p$ -values of the estimated coefficients in Table 1.

The mean inter-spike interval was positively correlated with MER in degenerated RGCs; however, it was not in normal RGCs. In Figure 6B, the regression line (black dashed line) of normal RGCs shows a slightly positive correlation with MER. However, this positive relationship was not statistically significant in normal RGCs (n.s., Table 1). In contrast, the regression line (red dashed line) of degenerated RGCs showed a strong positive correlation with MER, which was statistically significant ( $***p < 0.001$ ; Table 1). The estimated coefficient of the mean ISI was 0.0012 (Table 1).

Similarly, the SD of the ISI was positively correlated with MER only in degenerated RGCs but not in normal RGCs. In Figure 6C, the regression line (black dashed line) of normal RGCs shows a slightly positive correlation with MER. However, this positive relationship was not statistically significant in normal RGCs (n.s., Table 1). In contrast, the regression line (red dashed line) of degenerated RGCs showed a stronger positive correlation with MER, which was statistically significant ( $*p < 0.05$ , Table 1).

The CV of the ISI was negatively correlated with MER only in degenerated RGCs but not in normal RGCs. In Figure 6D, the regression line (black dashed line) of normal RGCs shows a slightly negative correlation with MER. However, this negative relationship was not statistically significant in normal RGCs (n.s., Table 1). In contrast, the regression line (red dashed line) of the degenerated RGCs showed a stronger negative correlation with MER, which was statistically significant ( $**p < 0.01$ ; Table 1).

Figure 7 shows the histograms of the ISI of RGCs with low (A) and high (B) modulation efficiencies. The ISI of normal RGCs showed a single peak at a very small value and decayed rapidly at larger values at both low and high MER (Figures 7A, B). This shape fits with the gamma distribution (black dashed curves). In contrast, the ISI histogram of degenerated RGCs showed an extra bump at approximately 50 ms (red triangles in Figure 7), which was more prominent at a higher MER (Figure 7B). The gamma and

normal distribution mixtures fit the multimodal histograms (dashed red curves).

## 4 Discussion

Previous studies on the effective activation of RGCs using electrical stimulation have significantly advanced our understanding of retinal prostheses. These investigations have explored various aspects of electrical stimulation, including electrode design, stimulation parameters, and the intricacies of RGC responses to electrical pulses (Jensen et al., 2003; Jensen et al., 2005; Fried et al., 2006; Jensen and Rizzo, 2008; Sekirnjak et al., 2008; Jensen and Rizzo, 2009; Goo et al., 2011a; Habib et al., 2013; Jepson et al., 2013; Abramian et al., 2014; Ahn et al., 2015; Weitz et al., 2015; Ahn et al., 2022; Ahn et al., 2023; Cha et al., 2023; Gogliettino et al., 2023; Seo et al., 2024). The results of these studies provide critical insights into optimizing the efficacy of retinal prostheses to achieve precise and reliable activation of RGCs.

However, a simple comparison of different experiments cannot show how well electrical stimulation evokes RGC spikes. This study examines the physiological characteristics that may determine the efficiency of electrical stimulation and suggests that both external and internal variables play important roles in the MER.

### 4.1 MER is a reliable criterion for quantifying modulation efficiency

MER is a robust metric to quantify the efficiency of electrical stimulation in both normal and degenerated RGCs. MER is based on a statistically significant increase in post-stimulation firing rates compared with pre-stimulation firing rates measured in repeated trials. Therefore, MER is robust to the inherent variability in neural responses and experimental artifacts. More importantly, MER quantifies the electrical stimulation efficiency with a normalized value between zero and one for each RGC, whereas previous thresholding methods provided information about the threshold *per se* without distinguishing subtle differences in electrical stimulation efficiency. In general, the stimulation threshold is

defined as the stimulation setting that corresponds to a predefined (typically 50%) probability of eliciting an RGC spike (Cai et al., 2013; Boinagrov et al., 2014; Lorach et al., 2015). Another group defined the stimulation threshold as the current setting producing a > 90% probability of an RGC spike (Sekirnjak et al., 2006). In our previous study (Goo et al., 2011b; Cha et al., 2023), the efficiency of modulation was indirectly measured by interpolating the current amplitude of the stimulation, eliciting an RGC spike with a 50% probability. This approach is inherently unfavorable for a degenerated retina when quantifying modulation efficiency because a degenerated retina has fewer evoked RGC spikes per pulse than normal RGCs have. Consequently, the degenerated RGCs showed higher stimulation thresholds than the normal RGCs, regardless of the species (Cha et al., 2022; Ahn et al., 2023; Cha et al., 2023). The stimulation threshold provides information on the minimum intensity of electrical stimulation, which differs significantly between normal and degenerated RGCs.

In order to compare modulation efficiency ratios of different experiments, the stimulation amplitudes should be fixed. The MER would change for different choices of current amplitude values. This dependence of the modulation efficiency score on the specific choice of amplitude values could be reduced by using widely used current amplitude values. In our experiment, the safety limit determines the maximal current amplitude, resulting in a typical range of 0 to 100 uA. This study used nine current amplitude levels spread over 0~100 uA. For the lower current amplitude range (1~10 uA), more minute intervals of amplitudes were chosen (1, 5, and 10 uA). While for the higher current amplitude range (50~100 uA), more sparse intervals of amplitudes were chosen (50, 70, and 100 uA). This selection was based on the need to cover a wide range of amplitudes while ensuring safety and accuracy in our measurements.

The bimodal distribution of MER in both the normal and the degenerated RGCs (Figure 4B) supports the use of MER as a criterion for discriminating between high- and low-efficiency electrical modulation. The degenerated RGCs produced fewer spikes than the normal RGCs did in response to electrical stimulation at the same intensity, resulting in a lower average MER (Figure 4A). Nevertheless, the MER of the degenerated RGCs showed a bimodal distribution and a clear distinction between the high- and low-efficiency groups, demonstrating the feasibility of MER for analyzing individual RGCs. Therefore, MER is a reliable quantification criterion for both normal and degenerated RGCs.

We examined the external and internal variables related to MER to determine the conditions associated with higher modulation efficiency. The relationship between MER and external variables showed a similar trend for both normal and degenerated RGCs, but with different efficacies. A longer stimulation duration and shorter distance resulted in a higher electrical charge delivered to the RGCs, and as a result, a higher MER (Figure 5; Table 1). In contrast, internal variables were differentially associated with normal and degenerated RGCs. In the normal retina, internal variables did not affect MER (Figure 6; Table 1). Three internal variables (mean ISI, SD of ISI, and CV of ISI) were significantly associated with MER in the degenerated retinas. Among the three internal variables, the mean ISI is the most important. RGCs with relatively longer mean ISIs showed less hyperactivity. Therefore, they may serve as suitable targets for electrical stimulation.

## 4.2 Spontaneous firing of RGC spikes between normal and degenerated retinas

Spontaneous hyperactivity in RGCs is a well-known characteristic of degenerate retinas (Goo et al., 2011a; Sekirnjak et al., 2011; Stasheff et al., 2011; Soto et al., 2012; Yee et al., 2012; Margolis et al., 2014). Hyperactive firing of spontaneous RGC spikes has been observed in a genetic model and an n-methyl-n-nitrosourea (MNU)-induced degeneration mouse model (Tao et al., 2015). NHPs are ideal animal models because of their anatomical and physiological similarities to humans. However, a genetic model of retinal degeneration in primates is lacking. Iatrogenic NHP retinal degeneration (RD) models have been developed using chemical- and laser-induced methods (Shirai et al., 2016; Ou et al., 2018; Dhakal et al., 2020; McGregor et al., 2020; Choi et al., 2023).

Our previous NHP RD model study reported that spontaneous RGC spike firing in monkeys with MNU-induced RD was significantly higher than that in normal monkeys (Ahn et al., 2022).

However, in the present study, spontaneous RGC spike firing in normal and RD primates was not significantly different (Figure 2A).

There are several possible explanations for this disparity in results. One of the most important possibilities is the selection of RGCs. In our previous study, we counted the RGC in the pool when it showed a typical RGC spike form, as shown in Figure 1A of Ahn et al. (2022). We excluded the RGC in a normal retina if it fires spikes extraordinarily high. However, in this study, we counted all the RGCs even if they fired too many spontaneous spikes because we observed spontaneous hyperactive firing from patch to patch, not scarcely in normal retinas. In addition, we attempted to exclude any experimenter-based bias in cell pooling. Second, more animals and retinal patches were used in this study (animal number: normal = 3, RD = 3; retinal patch number: normal = 5, RD = 4) than in the previous study (animal number: normal = 3, RD = 2; retinal patch number: normal = 3, RD = 2). Additional animals and retinal patches can provide more objective findings. Third, the MNU-induced morphological changes in the outer nuclear layer, as confirmed by OCT findings [Figure 2 in Cha et al. (2023)] looked similar. However, degeneration-induced network changes in secondary neurons (such as bipolar and horizontal cells) were not the same in each RD case, inevitably resulting in different RGC spike firing patterns.

## 4.3 Difference in the mean ISI between normal and degenerated retinas

In this study, the responses of RGCs were summed, and their subtypes were not differentiated. Visual stimulus-driven classification should be performed to differentiate the RGC subtypes. Because we did not apply a visual stimulus for this experiment, we pooled all RGCs identified through spike waveform sorting without differentiating the RGC types.

Our ISI profile of the normal retinas showed a more heterogeneous distribution than that of the RD retinas (Figure 3). As proposed in our previous publication using an *rd10* mouse (Cha et al., 2022), if the ON response is preserved for longer than the OFF response with MNU-induced RD, more ON cells could remain. This

ON dominance leads to a more homogeneous distribution in the RD ISI profile. Previous primate research has focused only on the direct response of RGC regarding retinal prosthesis (Sekirnjak et al., 2008; Jepson et al., 2013; Gogliettino et al., 2023). Because our RGC spikes were derived from indirect network-mediated responses rather than direct responses, there may be a difference in RGC responses to electrical stimulation. During RD, there is a significant rewiring of synaptic connections in the inner retina (Marc et al., 2003). Gap junctions are essential for the generation of abnormal rhythmic bursts and oscillations in *rd10* RGCs (Toychiev et al., 2013; Menzler et al., 2014; Ivanova et al., 2016). Gap junction coupling between AII amacrine cells and ON-cone BCs is known to be involved in oscillation generation (Trenholm et al., 2012; Yee et al., 2012; Choi et al., 2014). These complex changes could affect the mean ISI in primates with RD.

We could better understand cell-type-specific responses if we linked the RGC subtype identified with the visual stimulus and each RGC subtype's response to electrical stimulation. This issue will be addressed in future studies.

#### 4.4 Effect of external variables on MER between normal and degenerated retinas

This study investigated the effects of two external variables, stimulation pulse duration and inter-electrode distance, on MER.

A more prolonged stimulation pulse significantly increased the MER in normal and RD retinas (Figure 5A). This can be easily explained by the two-fold increase in the charge applied to the retina. However, MER still falls under the MER value of 3.5/9 in the RD retina. These findings are compatible with our previous report [Figure 5 of Cha et al. (2023)], in that in RD retina, the evoked spikes of RGC barely cross the threshold value (0.5). They were consistently below the levels of the normal retina across all current amplitudes tested.

The MER in both the normal and RD retinas showed an inverse linear relationship with increased inter-electrode distance. The decrease in modulation efficiency with increasing interelectrode distance is consistent with the intuition that distant RGCs receive less electrical charge and, therefore, have a lower MER (Figure 5B).

An inversely linear curve along the inter-electrode distance in the RD retina seems to contradict the normalized RGC response with the distance between stimulation and recording electrodes in RD macaques [Figure 4C of Ahn et al. (2022)], which shows a widespread distribution of electrically evoked RGC populations. In this study, the MER was derived from the RGC response with nine different amplitudes tested and not from each current amplitude, as shown in Figure 4C of Ahn et al. (2022). If we integrate all the current amplitudes (10, 30, and 50  $\mu$ A), the previous Figure 4C of RD macaque could be similarly incorporated with our current Figure 5.

#### 4.5 Effect of internal variables on MER between normal and degenerated retinas

This study examined the effects of four internal variables, spontaneous firing rates, mean of ISI, SD of ISI, and CV of ISI,

on MER. Among the four internal variables, the statistic of ISI was significantly associated with the MER of degenerated RGCs. Specifically, degenerated RGCs with shorter ISIs tended to have lower MER (Figure 6B).

Degenerated RGCs showed a bump of around 50 ms in the ISI histogram (Figure 7). A possible physiological mechanism that generated this bump is the oscillatory membrane potential of degenerated RGCs. The origin of this oscillation is the electrical coupling between ON bipolar cells and AII amacrine cells in the degenerated retina (Borowska et al., 2011; Choi et al., 2014; Trenholm and Awatramani, 2015), which is supported by empirical evidence that gap junction blockers abolish such rhythmic activity of degenerated RGCs in mice. The same phenomenon has been observed in drug-induced retinal degeneration in rabbits (Ahn et al., 2019) and macaques (Ahn et al., 2022). Specifically, in Figure 1D of Ahn et al. (2022), the power spectral density of the local field potential of degenerated macaque RGCs showed a strong peak around 20 Hz, which corresponds to the bump around 50 ms in the inter-spike interval in our experiment.

A novel contribution of our study is that the degenerated RGCs with lower modulation efficiency tend to have shorter ISIs than 50 ms (~20 Hz). The synchronous firing around 20 Hz is the hallmark of degenerated RGCs. Our results show that there are degenerated RGCs that have prominent oscillatory spikes but still have higher modulation efficiency (Figure 7B). This suggests that more careful studies should be performed to dissociate the effects of oscillatory spikes driven by the electrical coupling and hyperactivity on a shorter time scale. Understanding the physiological mechanisms of the low modulation efficiency of hyperactive RGCs is an important future work. The modulation efficiency of the generated RGCs could be improved by suppressing the oscillatory drive from AII amacrine cells or by reducing the hyperactivity of the RGC itself.

#### 4.6 Feasibility of MER for *in vitro* MEA recording and clinical setting

We selected the stimulation channel in the middle of the MEA, considering the voltage gradient produced around the recording channel. Based on our results, we propose the following strategy for selecting the optimal stimulation channel for *in vitro* MEA recordings: First, record spontaneous RGC activity from all available channels of the MEA without electrical stimulation for a sufficient period (e.g., 30 s). Second, perform spike-sorting to obtain spontaneous spikes from individual RGCs. Third, calculate the mean ISIs of RGCs over a short time interval (e.g., 0.15 s) and identify RGCs with large mean ISI values. Fourth, identify candidate stimulation channels near RGCs with large mean ISIs. Finally, apply electrical stimulation to each candidate channel.

In this study, only one MEA channel was used for stimulation. In such scenarios, selecting the channel closest to the RGCs with the largest mean ISI is a promising strategy. Electrical stimulation can be simultaneously applied to multiple channels (Ryu et al., 2017). The spatial arrangement of candidate channels and the average ISIs of RGCs around the channels should be considered for multichannel stimulation to maximize modulation efficiency. Moreover, the

results of this study may also have implications for more advanced devices. For instance, the CMOS MEA, with a high spatial resolution, is used to investigate the functional properties of the retinal network (Stutzki et al., 2016; Cojocaru et al., 2022). Considering the ISI of RGCs and their spatial arrangement in such a setup could improve electrical stimulation efficiency.

We propose that the MER can be one method for calibrating retinal prostheses. Several uncertainties and challenges arise when an MEA device is implanted into a living retina. For example, an immune response may lead to inflammation and gliosis near the implanted device, and the displacement or corrosion of the MEA device can change the quality of the signal. Our results showed that the response of RGCs to electrical stimulation can be predicted based on the MER.

Therefore, the MER can be used to optimize the selection of stimulation channels for *in vitro* MEA experiments and practical calibration methods to achieve higher efficiency when testing retinal prostheses.

## 4.7 Conclusion

Quantifying the effective activation of RGCs by electrical stimulation is a bottleneck in the study of retinal prostheses under diverse experimental conditions. Therefore, we proposed a robust indicator, the MER, to assess the modulation efficiency of RGCs. To our knowledge, this is the first study to directly compare the responses of normal and degenerated primate RGCs to electrical stimulation, based on a common criterion. We selected two external variables (stimulation duration and inter-electrode distance) and four internal variables (spontaneous firing rate, the mean ISI, SD of ISI, and CV of ISI) as predictors of MER in normal and degenerated primate RGCs. Two external variables significantly affected the MER in normal and degenerated RGC ( $p < 0.05$ ). Three internal variables, such as the mean ISI, SD of ISI, and CV of ISI, significantly affected MER ( $p < 0.05$ ) in degenerated RGC but not in normal RGC. The most important variable affecting MER was the mean ISI. A shorter ISI indicates hyperactive firing in the degenerated retina, which prevents electrical stimulation from evoking more RGCs. We believe that this difference in spontaneous firing in the RD results in a lower MER than that in the normal retina. Selective recruitment of a less hyperactive RGC group in RD with electrical stimulation could significantly improve the efficacy of the retinal prosthesis.

In future research, exploring additional modulation-efficiency predictors will be helpful. A broader range of variables should be considered in future studies, including cell type, morphology, and genetic markers and their relationships with MER. This comprehensive approach may provide a more detailed understanding of RGC modulation. In addition, *in vivo* studies are required to further understand the modulation efficiency and improve the efficacy of retinal prostheses. Such studies are essential for assessing the complex dynamics of the living retina and the long-term viability of retinal implants. We expect MER to be a common feature when comparing RGC responses in both *in vitro* and *in vivo* experiments.

## Data availability statement

The raw data supporting the conclusions of this article will be made available by the authors, without undue reservation.

## Ethics statement

The animal study was approved by the Institutional Animal Care and Use Committee of Osong Medical Innovation Foundation, Cheongju, Republic of Korea (KBIO-IACUC-2020-054-4). The study was conducted in accordance with the local legislation and institutional requirements.

## Author contributions

YY: Conceptualization, Formal Analysis, Validation, Writing—original draft, Writing—review and editing, Data curation, Software, Visualization. SC: Conceptualization, Data curation, Formal Analysis, Validation, Writing—original draft, Investigation, Methodology, Visualization. YSG: Conceptualization, Data curation, Formal Analysis, Validation, Writing—original draft, Funding acquisition, Supervision, Visualization, Writing—review and editing.

## Funding

The authors declare that financial support was received for the research, authorship, and/or publication of this article. This research was funded by a grant from the National Research Foundation (NRF) of the Ministry of Science and ICT (MSIP) of South Korea (NRF-2022R1A2C2004793).

## Acknowledgments

All the authors thank Dae Jin Park for providing a valuable discussion.

## Conflict of interest

The authors declare that the research was conducted in the absence of any commercial or financial relationships that could be construed as a potential conflict of interest.

## Publisher's note

All claims expressed in this article are solely those of the authors and do not necessarily represent those of their affiliated organizations, or those of the publisher, the editors and the reviewers. Any product that may be evaluated in this article, or claim that may be made by its manufacturer, is not guaranteed or endorsed by the publisher.

## References

- Abramian, M., Lovell, N. H., Habib, A., Morley, J. W., Suaning, G. J., and Dokos, S. (2014). Quasi-monopolar electrical stimulation of the retina: a computational modelling study. *J. Neural Eng.* 11, 025002. doi:10.1088/1741-2560/11/2/025002
- Ahn, S. M., Ahn, J., Cha, S., Yun, C., Park, T. K., Goo, Y. S., et al. (2019). Development of a post-vitreotomy injection of N-methyl-N-nitrosourea as a localized retinal degeneration rabbit model. *Exp. Neurobiol.* 28, 62–73. doi:10.5607/en.2019.28.1.62
- Ahn, J., Cha, S., Choi, K. E., Kim, S. W., Yoo, Y., and Goo, Y. S. (2022). Correlated activity in the degenerate retina inhibits focal response to electrical stimulation. *Front. Cell Neurosci.* 16, 889663. doi:10.3389/fncel.2022.889663
- Ahn, J., Choi, M. H., Kim, K., Senok, S. S., Cho, D. D., Koo, K. I., et al. (2017). The advantage of topographic prominence-adopted filter for the detection of short-latency spikes of retinal ganglion cells. *Korean J. Physiol. Pharmacol.* 21, 555–563. doi:10.4196/kjpp.2017.21.5.555
- Ahn, J., Jeong, Y., Cha, S., Lee, J. Y., Yoo, Y., and Goo, Y. S. (2023). High amplitude pulses on the same charge condition efficiently elicit bipolar cell-mediated retinal ganglion cell responses in the degenerate retina. *Biomed. Eng. Lett.* 13, 129–140. doi:10.1007/s13534-023-00260-4
- Ahn, K. N., Ahn, J. Y., Kim, J. H., Cho, K., Koo, K. I., Senok, S. S., et al. (2015). Effect of stimulus waveform of biphasic current pulse on retinal ganglion cell responses in retinal degeneration (rd1) mice. *Korean J. Physiol. Pharmacol.* 19, 167–175. doi:10.4196/kjpp.2015.19.2.167
- Ahuja, A. K., Behrend, M. R., Kuroda, M., Humayun, M. S., and Weiland, J. D. (2008). An *in vitro* model of a retinal prosthesis. *IEEE Trans. Biomed. Eng.* 55, 1744–1753. doi:10.1109/tbme.2008.919126
- Ayton, L. N., Barnes, N., Dagnelie, G., Fujikado, T., Goetz, G., Hornig, R., et al. (2020). An update on retinal prostheses. *Clin. Neurophysiol.* 131, 1383–1398. doi:10.1016/j.clinph.2019.11.029
- Boinagrov, D., Pangratz-Fuehrer, S., Goetz, G., and Palanker, D. (2014). Selectivity of direct and network-mediated stimulation of the retinal ganglion cells with epi-sub- and intraretinal electrodes. *J. Neural Eng.* 11, 026008. doi:10.1088/1741-2560/11/2/026008
- Borowska, J., Trenholm, S., and Awatramani, G. B. (2011). An intrinsic neural oscillator in the degenerating mouse retina. *J. Neurosci.* 31, 5000–5012. doi:10.1523/JNEUROSCI.5800-10.2011
- Cai, C., Twyford, P., and Fried, S. (2013). The response of retinal neurons to high-frequency stimulation. *J. Neural Eng.* 10, 036009. doi:10.1088/1741-2560/10/3/036009
- Cha, S., Ahn, J., Jeong, Y., Lee, Y. H., Kim, H. K., Lee, D., et al. (2022). Stage-Dependent changes of visual function and electrical response of the retina in the rd10 mouse model. *Front. Cell Neurosci.* 16, 926096. doi:10.3389/fncel.2022.926096
- Cha, S., Ahn, J., Kim, S.-W., Choi, K.-E., Yoo, Y., Eom, H., et al. (2023). The variation of electrical pulse duration elicits reliable network-mediated responses of retinal ganglion cells in normal, not in degenerate primate retinas. *Bioengineering* 10, 1135. doi:10.3390/bioengineering10101135
- Choi, H., Zhang, L., Cembrowski, M. S., Sabottke, C. F., Markowitz, A. L., Butts, D. A., et al. (2014). Intrinsic bursting of AII amacrine cells underlies oscillations in the rd1 mouse retina. *J. Neurophysiol.* 112, 1491–1504. doi:10.1152/jn.00437.2014
- Choi, K. E., Cha, S., Yun, C., Ahn, J., Hwang, S., Kim, Y. J., et al. (2023). Outer retinal degeneration in a non-human primate model using temporary intravitreal tamponade with N-methyl-N-nitrosourea in cynomolgus monkeys. *J. Neural Eng.* 20, 015001. doi:10.1088/1741-2552/acb085
- Cojocaru, A. E., Corna, A., Reh, M., and Zeck, G. (2022). High spatial resolution artificial vision inferred from the spiking output of retinal ganglion cells stimulated by optogenetic and electrical means. *Front. Cell Neurosci.* 16, 1033738. doi:10.3389/fncel.2022.1033738
- Dayan, P., and Abbott, L. F. (2005). *Theoretical neuroscience: computational and mathematical modeling of neural systems*. Cambridge: MIT press, 24–34.
- Dempster, A. P., Laird, N. M., and Rubin, D. B. (1977). Maximum likelihood from incomplete data via the EM algorithm. *J. R. Stat. Soc. Ser. B Methodol.* 39, 1–22. doi:10.1111/j.2517-6161.1977.tb01600.x
- Dhakal, K. R., Walters, S., Mcgregor, J. E., Schwarz, C., Strazzeri, J. M., Aboulizadeh, E., et al. (2020). Localized photoreceptor ablation using femtosecond pulses focused with adaptive optics. *Transl. Vis. Sci. Technol.* 9, 16. doi:10.1167/tvst.9.7.16
- Eickenscheidt, M., Jenkner, M., Thewes, R., Fromherz, P., and Zeck, G. (2012). Electrical stimulation of retinal neurons in epiretinal and subretinal configuration using a multielectrode array. *J. Neurophysiol.* 107, 2742–2755. doi:10.1152/jn.00909.2011
- Freeman, D. K., Rizzo, J. F., and Fried, S. I. (2010). Electric stimulation with sinusoids and white noise for neural prostheses. *Front. Neurosci.* 4, 28. doi:10.3389/fncel.2010.001.2010
- Fried, S. I., Hsueh, H. A., and Werblin, F. S. (2006). A method for generating precise temporal patterns of retinal spiking using prosthetic stimulation. *J. Neurophysiol.* 95, 970–978. doi:10.1152/jn.00849.2005
- Fujikado, T., Kamei, M., Sakaguchi, H., Kanda, H., Endo, T., Hirota, M., et al. (2016). One-year outcome of 49-channel suprachoroidal-transretinal stimulation prosthesis in patients with advanced retinitis pigmentosa. *Invest. Ophthalmol. Vis. Sci.* 57, 6147–6157. doi:10.1167/iov.16-20367
- Gogliettino, A. R., Madugula, S. S., Grosberg, L. E., Vilku, R. S., Brown, J., Nguyen, H., et al. (2023). High-fidelity reproduction of visual signals by electrical stimulation in the central primate retina. *J. Neurosci.* 43, 4625–4641. doi:10.1523/JNEUROSCI.1091-22.2023
- Goo, Y. S., Ahn, K. N., Song, Y. J., Ahn, S. H., Han, S. K., Ryu, S. B., et al. (2011a). Spontaneous oscillatory rhythm in retinal activities of two retinal degeneration (rd1 and rd10) mice. *Korean J. Physiol. Pharmacol.* 15, 415–422. doi:10.4196/kjpp.2011.15.6.415
- Goo, Y. S., Park, D. J., Ahn, J. R., and Senok, S. S. (2016). Spontaneous oscillatory rhythms in the degenerating mouse retina modulate retinal ganglion cell responses to electrical stimulation. *Front. Cell Neurosci.* 9, 512. doi:10.3389/fncel.2015.00512
- Goo, Y. S., Ye, J. H., Lee, S., Nam, Y., Ryu, S. B., and Kim, K. H. (2011b). Retinal ganglion cell responses to voltage and current stimulation in wild-type and rd1 mouse retinas. *J. Neural Eng.* 8, 035003. doi:10.1088/1741-2560/8/3/035003
- Grosberg, L. E., Ganesan, K., Goetz, G. A., Madugula, S. S., Bhaskhar, N., Fan, V., et al. (2017). Activation of ganglion cells and axon bundles using epiretinal electrical stimulation. *J. Neurophysiol.* 118, 1457–1471. doi:10.1152/jn.00750.2016
- Habib, A. G., Cameron, M. A., Suaning, G. J., Lovell, N. H., and Morley, J. W. (2013). Spatially restricted electrical activation of retinal ganglion cells in the rabbit retina by hexapolar electrode return configuration. *J. Neural Eng.* 10, 036013. doi:10.1088/1741-2560/10/3/036013
- Humayun, M. S., Dorn, J. D., Da Cruz, L., Dagnelie, G., Sahel, J. A., Stanga, P. E., et al. (2012). Interim results from the international trial of Second Sight's visual prosthesis. *Ophthalmology* 119, 779–788. doi:10.1016/j.ophtha.2011.09.028
- Ivanova, E., Yee, C. W., Baldoni, R., Jr., and Sagdullaev, B. T. (2016). Aberrant activity in retinal degeneration impairs central visual processing and relies on Cx36-containing gap junctions. *Exp. Eye Res.* 150, 81–89. doi:10.1016/j.exer.2015.05.013
- Jain, A. K. (2010). Data clustering: 50 years beyond K-means. *Pattern Recognit. Lett.* 31, 651–666. doi:10.1016/j.patrec.2009.09.011
- Jensen, R. J., and Rizzo, J. F. (2008). Activation of retinal ganglion cells in wild-type and rd1 mice through electrical stimulation of the retinal neural network. *Vis. Res.* 48, 1562–1568. doi:10.1016/j.visres.2008.04.016
- Jensen, R. J., and Rizzo, J. F. (2009). Activation of ganglion cells in wild-type and rd1 mouse retinas with monophasic and biphasic current pulses. *J. Neural Eng.* 6, 035004. doi:10.1088/1741-2560/6/3/035004
- Jensen, R. J., Rizzo, J. F., 3rd, Ziv, O. R., Grumet, A., and Wyatt, J. (2003). Thresholds for activation of rabbit retinal ganglion cells with an ultrafine, extracellular microelectrode. *Invest. Ophthalmol. Vis. Sci.* 44, 3533–3543. doi:10.1167/iov.02-1041
- Jensen, R. J., Ziv, O. R., and Rizzo, J. F. (2005). Thresholds for activation of rabbit retinal ganglion cells with relatively large, extracellular microelectrodes. *Invest. Ophthalmol. Vis. Sci.* 46, 1486–1496. doi:10.1167/iov.04-1018
- Jepson, L. H., Hottowy, P., Mathieson, K., Gunning, D. E., Dabrowski, W., Litke, A. M., et al. (2013). Focal electrical stimulation of major ganglion cell types in the primate retina for the design of visual prostheses. *J. Neurosci.* 33, 7194–7205. doi:10.1523/JNEUROSCI.4967-12.2013
- Lorach, H., Goetz, G., Smith, R., Lei, X., Mandel, Y., Kamins, T., et al. (2015). Photovoltaic restoration of sight with high visual acuity. *Nat. Med.* 21, 476–482. doi:10.1038/nm.3851
- Macqueen, J. (1967). "Some methods for classification and analysis of multivariate observations," in Proceedings of the fifth Berkeley symposium on mathematical statistics and probability, Oakland, CA, USA, 281–297.
- Madugula, S. S., Gogliettino, A. R., Zaidi, M., Aggarwal, G., Kling, A., Shah, N. P., et al. (2022). Focal electrical stimulation of human retinal ganglion cells for vision restoration. *J. Neural Eng.* 19, 066040. doi:10.1088/1741-2552/aca5b5
- Marc, R. E., Jones, B. W., Watt, C. B., and Strettoi, E. (2003). Neural remodeling in retinal degeneration. *Prog. Retin Eye Res.* 22, 607–655. doi:10.1016/s1350-9462(03)00039-9
- Margolis, D. J., Gartland, A. J., Singer, J. H., and Detwiler, P. B. (2014). Network oscillations drive correlated spiking of ON and OFF ganglion cells in the rd1 mouse model of retinal degeneration. *PLoS One* 9, e86253. doi:10.1371/journal.pone.0086253
- Mcgregor, J. E., Godat, T., Dhakal, K. R., Parkins, K., Strazzeri, J. M., Bateman, B. A., et al. (2020). Optogenetic restoration of retinal ganglion cell activity in the living primate. *Nat. Commun.* 11, 1703. doi:10.1038/s41467-020-15317-6
- Menzler, J., Channappa, L., and Zeck, G. (2014). Rhythmic ganglion cell activity in bleached and blind adult mouse retinas. *PLoS One* 9, e106047. doi:10.1371/journal.pone.0106047
- Otsu, N. (1979). A threshold selection method from gray-level histograms. *IEEE Trans. Syst. Man, Cybern.* 9, 62–66. doi:10.1109/tsmc.1979.4310076
- Ou, Q., Zhu, T., Li, P., Li, Z., Wang, L., Lian, C., et al. (2018). Establishment of retinal degeneration model in rat and monkey by intravitreal injection of sodium iodate. *Curr. Mol. Med.* 18, 352–364. doi:10.2174/1566524018666181113104023

- Parsons, O. E. (2020). "A Gaussian mixture model approach to classifying response types," in *Mixture models and applications*. Editors N. Bouguila and W. Fan (Berlin: Springer), 3–22.
- Ryu, S. B., Choi, J. W., Ahn, K. N., Goo, Y. S., and Kim, K. H. (2017). Amplitude modulation-based electrical stimulation for encoding multipixel spatiotemporal visual information in retinal neural activities. *J. Korean Med. Sci.* 32, 900–907. doi:10.3346/jkms.2017.32.6.900
- Sekirnjak, C., Hottowy, P., Sher, A., Dabrowski, W., Litke, A. M., and Chichilnisky, E. J. (2006). Electrical stimulation of mammalian retinal ganglion cells with multielectrode arrays. *J. Neurophysiol.* 95, 3311–3327. doi:10.1152/jn.01168.2005
- Sekirnjak, C., Hottowy, P., Sher, A., Dabrowski, W., Litke, A. M., and Chichilnisky, E. J. (2008). High-resolution electrical stimulation of primate retina for epiretinal implant design. *J. Neurosci.* 28, 4446–4456. doi:10.1523/JNEUROSCI.5138-07.2008
- Sekirnjak, C., Jepson, L. H., Hottowy, P., Sher, A., Dabrowski, W., Litke, A. M., et al. (2011). Changes in physiological properties of rat ganglion cells during retinal degeneration. *J. Neurophysiol.* 105, 2560–2571. doi:10.1152/jn.01061.2010
- Seo, H. W., Cha, S., Jeong, Y., Ahn, J., Lee, K. J., Kim, S., et al. (2024). Focal stimulation of retinal ganglion cells using subretinal 3D microelectrodes with peripheral electrodes of opposite current. *Biomed. Eng. Lett.* 14, 355–365. doi:10.1007/s13534-023-00342-3
- Shirai, H., Mandai, M., Matsushita, K., Kuwahara, A., Yonemura, S., Nakano, T., et al. (2016). Transplantation of human embryonic stem cell-derived retinal tissue in two primate models of retinal degeneration. *Proc. Natl. Acad. Sci. U. S. A.* 113, E81–E90. doi:10.1073/pnas.1512590113
- Soto, F., Ma, X., Cecil, J. L., Vo, B. Q., Culican, S. M., and Kerschensteiner, D. (2012). Spontaneous activity promotes synapse formation in a cell-type-dependent manner in the developing retina. *J. Neurosci.* 32, 5426–5439. doi:10.1523/JNEUROSCI.0194-12.2012
- Stasheff, S. F., Shankar, M., and Andrews, M. P. (2011). Developmental time course distinguishes changes in spontaneous and light-evoked retinal ganglion cell activity in rd1 and rd10 mice. *J. Neurophysiol.* 105, 3002–3009. doi:10.1152/jn.00704.2010
- Stingl, K., Bartz-Schmidt, K. U., Besch, D., Chee, C. K., Cottrill, C. L., Gekeler, F., et al. (2015). Subretinal visual implant alpha IMS--clinical trial interim report. *Vis. Res.* 111, 149–160. doi:10.1016/j.visres.2015.03.001
- Stutzki, H., Helmhold, F., Eickenscheidt, M., and Zeck, G. (2016). Subretinal electrical stimulation reveals intact network activity in the blind mouse retina. *J. Neurophysiol.* 116, 1684–1693. doi:10.1152/jn.01095.2015
- Tao, Y., Chen, T., Fang, W., Peng, G., Wang, L., Qin, L., et al. (2015). The temporal topography of the N-Methyl- N-nitrosourea induced photoreceptor degeneration in mouse retina. *Sci. Rep.* 5, 18612. doi:10.1038/srep18612
- Toychiev, A. H., Ivanova, E., Yee, C. W., and Sagdullaev, B. T. (2013). Block of gap junctions eliminates aberrant activity and restores light responses during retinal degeneration. *J. Neurosci.* 33, 13972–13977. doi:10.1523/JNEUROSCI.2399-13.2013
- Trenholm, S., and Awatramani, G. B. (2015). Origins of spontaneous activity in the degenerating retina. *Front. Cell. Neurosci.* 9, 277. doi:10.3389/fncel.2015.00277
- Trenholm, S., Borowska, J., Zhang, J. W., Hoggarth, A., Johnson, K., Barnes, S., et al. (2012). Intrinsic oscillatory activity arising within the electrically coupled AII amacrine-ON cone bipolar cell network is driven by voltage-gated Na<sup>+</sup> channels. *J. Physiology-London* 590, 2501–2517. doi:10.1113/jphysiol.2011.225060
- Twyford, P., and Fried, S. (2016). The retinal response to sinusoidal electrical stimulation. *IEEE Trans. Neural Syst. Rehabil. Eng.* 24, 413–423. doi:10.1109/TNSRE.2015.2415811
- Weiland, J. D., Walston, S. T., and Humayun, M. S. (2016). Electrical stimulation of the retina to produce artificial vision. *Annu. Rev. Vis. Sci.* 2, 273–294. doi:10.1146/annurev-vision-111815-114425
- Weitz, A. C., Behrend, M. R., Lee, N. S., Klein, R. L., Chiodo, V. A., Hauswirth, W. W., et al. (2013). Imaging the response of the retina to electrical stimulation with genetically encoded calcium indicators. *J. Neurophysiol.* 109, 1979–1988. doi:10.1152/jn.00852.2012
- Weitz, A. C., Nanduri, D., Behrend, M. R., Gonzalez-Calle, A., Greenberg, R. J., Humayun, M. S., et al. (2015). Improving the spatial resolution of epiretinal implants by increasing stimulus pulse duration. *Sci. Transl. Med.* 7, 318ra203. doi:10.1126/scitranslmed.aac4877
- Xu, L., and Jordan, M. I. (1996). On convergence properties of the EM algorithm for Gaussian mixtures. *Neural Comput.* 8, 129–151. doi:10.1162/neco.1996.8.1.129
- Yee, C. W., Toychiev, A. H., and Sagdullaev, B. T. (2012). Network deficiency exacerbates impairment in a mouse model of retinal degeneration. *Front. Syst. Neurosci.* 6, 8. doi:10.3389/fnsys.2012.00008